A FINITE ELEMENT MODEL FOR COMPOSITE BEAMS WITH PIEZOELECTRIC LAYERS USING A SINUS MODEL

S.B. Beheshti-Aval * **M. Lezgy-Nazargah** **

Department of Civil Engineering
Khajeh Nasir Toosi University of Technology (KNTU)
Tehran, Iran

ABSTRACT

In this study, finite element modeling of composite beams with distributed piezoelectric sensors and actuators which is based upon a coupled electromechanical model has been considered. For modeling of mechanical displacement through the thickness, a sinus model that satisfies continuity conditions of transverse shear stresses and the boundary conditions on the upper and lower surfaces of the beam has been employed. In the presented model, the number of unknowns is not dependent on the number of layers. The variation of electric potential in each piezoelectric layer has been modeled using layer-wise theory. By applying the virtual work principle (VWP), a formulation has been developed for a two-nodded Hermitian-2(n + 1) layer-wise nodded element for a n-layered beam. The VWP leads to a derivation that could include dynamic analysis. However, in this study only static problems have been considered. Comparison of results obtained from this formulation with available works in the literature, demonstrates efficiency of proposed model in analysis of laminated beams under mechanical and electrical loadings.

Keywords : Finite element, Composite beams, Piezoelectric layers, Sinus model, Transverse stress.

1. INTRODUCTION

In the past ten years, smart structures have attracted significant attention of many researchers in the field of active control and dynamic. By developing smart structures, piezoelectric materials have been used extensively as distributed sensors and actuators. The coupled electromechanical properties of piezoelectric materials and their lightness make them suitable for use in advanced smart structures. A piezoelectric material generates an electrical charge when subjected to a mechanical deformation (direct piezoelectric effect), and conversely, the piezoelectric material deforms when subjected to an electrical field (inverse piezoelectric effect). Therefore, piezoelectric materials are capable of acting as distributed sensors and actuators.

Various mathematical models have been presented to predict the behavior of structures containing piezoelectric sensors and actuators. These models can be classified into two broad groups: Induced strain models and coupled electromechanical models.

In the induced strain models, approximate theories have been employed to incorporate the piezoelectric effects [1-4]. In these models, the electric potential is neglected as a state variable in the formulation. However, the induced strain models encounter limitations that arise from the use of force approximation to represent the piezoelectric strains. This approximate representation is not able to capture the coupled mechanical and electrical response and limits these models only in predicting the actuator behavior of piezoelectric materials.

The coupled electromechanical models are able to predict both the sensor and actuator behavior of piezoelectric materials, due to incorporation both the displacements and electric potential as state variables in the formulation. Wu and his colleagues used an analytical approach to obtain three-dimensional (3D) exact solutions of multilayered piezoelectric plates/shells. The formulation of these researchers is based on 3D piezoelectricity and the method of perturbation has been used in their derivations [5-7]. Some researchers used 3D finite element to analyze the structures containing piezoelectric sensors and actuators [8-10]. Although 3D finite element analysis gives accurate results, but requires huge computational effort. Moreover, the computational involvement becomes high when piezoelectric layers are too thin compared to the

* Assistant Professor, corresponding author ** Ph.D. student

main structure. This situation is quite common in many practical problems. Thus this kind of approach is inadequate in handling a real problem. In order to improve computational efficiency layer-wise theories were presented by Garcao *et al*. [11], Garcia Lage *et al*. [12,13], Heyliger and Saravanos [14], and Saravanos *et al*. [15]. In spite of the fact that layer-wise theories improve the computational efficiency, in these methods the number of unknowns are dependent on the number of layers. So, layer-wise theories are also rather expensive approaches. In order to overcome these limitations, the concept of mixed theory was presented [16,17]. In this theory, the modeling of mechanical components is based on single layer plate theory whereas electric potential is modeled with layer-wise theory. Because of using single layer theory for mechanical components in mixed theory, the number of unknowns is independent of the number of layers.

Because of expressing the variation of displacement components through the thickness by continuous functions, all the strain components obtained from single layer theory are continuous and all the stress components are discontinuous at the layer interfaces. In a laminated structure, in-plane strains and out of plane stresses are continuous at the layer interfaces whereas in-plane stresses and out of plane strains are discontinuous [18-20]. Therefore, single layer theory is not able to model the behavior of a composite structure properly.

In order to overcome the drawback of single layer theory, the idea of refined theory was presented by researchers [21,22]. First, refined first-order shear deformation theory (RFSDT) was presented. In RFSDT, the variation of in-plane displacement through the thickness of plate is piece-wise linear while transverse displacement is constant across the thickness. Bhaskar and Varadan [23], Di Scuiva [24], Lee and Liu [25], Parmerter and Cho [26] combined the concepts of RFSDT and high shear deformation theory (third-order SDT) of Reddy [27] to develop a new class of refined theory defined as refined higher order shear deformation theory (RHSDT). In RHSDT, the transverse shear stresses are continuous at the layer interfaces and have a piece-wise parabolic variation across the laminate thickness. The transverse stresses continuity ensures discontinuity of transverse strains at the interface of two layers which have different rigidity. Moreover, the transverse shear stresses satisfy the boundary conditions on the upper and lower surfaces. Distribution of potential electric in piezoelectric layers (actuators and/or sensors) is represented by the usual layer-wise theory.

In this study a new element has been proposed that has the same number of mechanical and electrical degree of freedom with mixed model of Chee *et al*. [28]. In comparison to their mixed model, our proposed formulation ensures continuity requirements of the transverse shear stresses. In our new model, the variation of mechanical displacement across the thickness is based on a sinus model [29]. This model satisfies free condition of the transverse shear stresses on the top and bottom surfaces of beam as well as continuity condition of the transverse shear stresses at the layer interfaces. It has only three independent generalized displacements: Two displacements and one rotation. It has C^0 continuity except for the transverse displacement associated with bending which has C^1. Concerning the electric potential, the through thickness variation is modeled by the usual layer-wise theory. A computer code whose algorithm is based on the presented model has been developed. Obtained numerical results show a good agreement with other published results.

2. BASIC PIEZOELECTRIC EQUATIONS AND VIRTUAL WORK PRINCIPLE [30]

The governing equations for a piezoelectric body of volume Ω and regular boundary surface S, can be written as:

$$\sigma_{ij,j} + f_i = \rho \ddot{u}_i \tag{1}$$

$$D_{i,i} - q = 0 \tag{2}$$

where, f_i, q, ρ, are mechanical body force components, electric body charge and mass density respectively. σ_{ij} and D_i are the symmetric Cauchy stress tensor and electric displacement components. The following converse and direct linear piezoelectric constitutive equations relate stress and electric displacement components to the linear symmetric Lagrange strain tensor components ε_{ij} and electric field components E_i:

$$\sigma_{ij} = C_{ijkl}\, \varepsilon_{kl} - e_{kij}\, E_k \tag{3}$$

$$D_i = e_{ikl}\, \varepsilon_{kl} + \chi_{ik}\, E_k \tag{4}$$

C_{ijkl}, e_{kij} and χ_{ik} denotes elastic, piezoelectric and dielectric material constants. The strain tensor and electric field components are obtained from mechanical displacements u_i and electric field potential ϕ through the following relations:

$$\varepsilon_{ij} = \frac{1}{2}(u_{i,j} + u_{j,i}) \tag{5}$$

$$E_i = -\phi_{,i} \tag{6}$$

Essential or natural mechanical and electrical boundary conditions or a combination of them must be satisfied on boundary surface S:

$$u_i = U_i \tag{7a}$$

or

$$\sigma_{ij}\, n_j = F_i \tag{7b}$$

$$\phi = V \tag{8a}$$

or

$$D_i\, n_i = -Q \tag{8b}$$

where U_i, F_i, V, Q and n_i are respectively prescribed mechanical displacement and surface force components, electric potential and surface charge, and outward unit normal vector components.

Using admissible virtual displacement δu_i and potential $\delta\phi$, Eqs. (1) and (2) give the following expression:

$$\int_\Omega (\sigma_{ij,j} + f_i - \rho\ddot{u}_i)\,\delta u_i\, d\Omega + \int_\Omega (D_{i,i} - q)\,\delta\phi\, d\Omega = 0 \qquad (9)$$

Integrating this equation by parts and using divergence theorem gives:

$$\begin{aligned} &-\int_\Omega \sigma_{ij}\,\delta u_{i,j}\, d\Omega + \int_S \sigma_{ij}\, n_j\, \delta u_i\, dS + \int_\Omega f_i\,\delta u_i\, d\Omega - \int_\Omega \rho\ddot{u}_i\,\delta u_i\, d\Omega \\ &-\int_\Omega D_i\,\delta\phi_{,i}\, d\Omega + \int_S D_i\, n_i\,\delta\phi\, dS - \int_\Omega q\,\delta\phi\, d\Omega = 0 \end{aligned} \qquad (10)$$

Using the symmetry property of the stress tensor, the natural boundary conditions (7b), (8b) and replacing the electric field-potential Eq. (6) into Eq. (10) leads to:

$$\begin{aligned} &-\int_\Omega \sigma_{ij}\,\delta\varepsilon_{ij}\, d\Omega + \int_S F_i\,\delta u_i\, dS + \int_\Omega f_i\,\delta u_i\, d\Omega + f_{ci}\,\delta u_i \\ &-\int_\Omega \rho\ddot{u}_i\,\delta u_i\, d\Omega + \int_\Omega D_i\,\delta E_i\, d\Omega - \int_S Q\,\delta\phi\, dS - \int_\Omega q\,\delta\phi\, d\Omega = 0 \end{aligned} \qquad (11)$$

where f_{ci} is the components of concentrated load.

3. MATHEMATICAL FORMULATION

3.1 Geometry and Coordinate System

In this study, the assumed composite beam is made of *NC* layers of different linearly elastic materials. It has a uniform rectangular cross section of height h, width b and its length is L. Each layer may be piezoelectric (actuator and/or sensor) or non-piezoelectric. In Fig. 1, the laminated beam has been shown in a Cartesian Coordinate System (x, y, z).

3.2 Constitutive Relations

Considering only bending about the y axis is taken into account, and the cross section is symmetric about the z axis, the constitutive equation of piezoelectric material in its material-axis system can be written as:

$$\sigma_s = C_s\,\varepsilon_s \qquad (12)$$

where

$$\sigma_s = [\sigma_1 \quad \sigma_5 \quad D_1 \quad D_3]$$

$$\varepsilon_s = [\varepsilon_1 \quad \varepsilon_5 \quad -E_1 \quad -E_3]$$

$$C_s = \begin{bmatrix} C & e \\ e^T & -\chi \end{bmatrix},$$

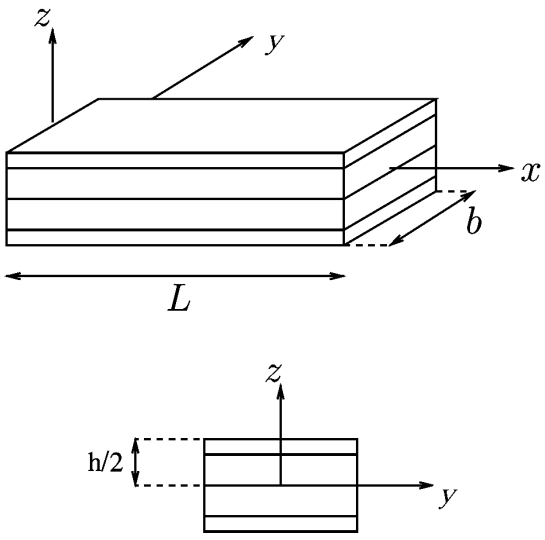

Fig. 1 The laminated beam and co-ordinate system

$$C = \begin{bmatrix} c_{11} - \dfrac{c_{13}^2}{c_{33}} & 0 \\ 0 & c_{55} \end{bmatrix}, \quad e = \begin{bmatrix} 0 & e_{31} - \dfrac{c_{13}\, e_{33}}{c_{33}} \\ e_{15} & 0 \end{bmatrix},$$

$$\chi = \begin{bmatrix} \chi_{11} & 0 \\ 0 & \chi_{33} + \dfrac{e_{33}^2}{c_{33}} \end{bmatrix}$$

In the above equations, σ_i and D_i are respectively the components of stress and electric displacement. ε_j and E_j are the components of strain and electric field respectively and c_{ij}, k_{ij} and e_{ij} are the corresponding elastic, permittivity and piezoelectric constants.

The constitutive equation of a lamina in a common structural axis system can be expressed as:

$$\bar{\sigma} = \bar{Q}\bar{\varepsilon} \qquad (13)$$

where

$$\bar{\sigma} = [\sigma_x \quad \tau_{xz} \quad D_x \quad D_z]^T$$

$$\bar{\varepsilon} = [\varepsilon_x \quad \gamma_{xz} \quad -E_x \quad -E_z]$$

$$\bar{Q} = T^T C_s\, T = \begin{bmatrix} \bar{C} & \bar{e} \\ \bar{e}^T & -\bar{\chi} \end{bmatrix}$$

In the above equation, T is the transformation matrix. In this work the non-piezoelectric materials is assumed to be orthotropic and the general type of piezoelectric materials is 'orthorhombic-class mm^2'.

3.3 Displacement and Strain Fields

The displacement field used in this model is given by [29]

$$U(x,\ z,\ t) = u(x,\ t) - z\frac{dw(x)}{dx} + \left(\frac{dw(x)}{dx} + \psi_x(x,\ t)\right)$$
$$\left\{f(z) + \sum_{i=1}^{(NC)-1} \alpha_i \left(-\frac{1}{2}z + \frac{1}{2}g(z) + (z - z_{i+1})H(z - z_{i+1})\right)\right\}$$
$$W(x,\ z,\ t) = w(x,\ t) \tag{14}$$

$U(x, z, t)$ and $W(x, z, t)$ are the horizontal and vertical displacements respectively. $u(x, t)$ and $w(x, t)$ are the mid-plane horizontal and vertical displacement respectively. $\psi_x(x, t)$ is the shear bending rotation around the z axis. H is Heaviside function, $f(z)$ and $g(z)$ are defined by

$$\begin{cases} f(z) = \dfrac{h}{\pi}\sin\left(\dfrac{\pi z}{h}\right) \\ f'(z) = \cos\left(\dfrac{\pi z}{h}\right) \end{cases} \qquad \begin{cases} g(z) = \dfrac{h}{\pi}\cos\left(\dfrac{\pi z}{h}\right) \\ g'(z) = -\sin\left(\dfrac{\pi z}{h}\right) \end{cases}$$

α_i are the continuity coefficients obtained from a linear system. The calculation of these coefficients is detailed in Section *A*. The coordinate system of laminated beam has been shown in Fig. 2.

Using the usual definition of strain (see Eq. (5)), the strain equations can be derived from Eq. (14) as follow:

$$\varepsilon_1 = \varepsilon_x = \frac{du}{dx} - z\frac{d^2w}{dx^2} + \left(\frac{d\psi_x}{dx^2} + \frac{d^2w}{dx^2}\right)F(z)$$
$$\varepsilon_5 = \gamma_{zx} = \left(\psi_x + \frac{dw}{dx}\right)S(z) \tag{15}$$

where

$$F(z) = f(z) + \sum_{i=1}^{(NC)-1} \alpha_i \left(-\frac{1}{2}z + \frac{1}{2}g(z) + (z - z_{i+1})H(z - z_{i+1})\right)$$
$$S(z) = f'(z) + \sum_{i=1}^{(NC)-1} \alpha_i \left(-\frac{1}{2} + \frac{1}{2}g'(z) + H(z - z_{i+1}) + (z - z_{i+1})\,\delta(z - z_{i+1})\right)$$

and $\delta(z - z_{i+1})$ is first derivative of $H(z - z_{i+1})$.

The strain and displacement Eqs. (14) and (15) can be expressed in the following matrix form:

$$u = A_u\, u_u\ , \quad \varepsilon = L_u\, u_u \tag{16}$$

where $u = [U\ \ W]^T$, $u_u = [u\ \ w\ \ \psi_x]^T$, $\varepsilon = [\varepsilon_1\ \ \varepsilon_5]^T$, and

$$A_u = \begin{bmatrix} 1 & -z\dfrac{d}{dx} + F(z)\dfrac{d}{dx} & F(z) \\ 0 & 1 & 0 \end{bmatrix},$$
$$L_u = \begin{bmatrix} \dfrac{d}{dx} & -z\dfrac{d^2}{dx^2} + F(z)\dfrac{d^2}{dx^2} & F(z)\dfrac{d}{dx} \\ 0 & S(z)\dfrac{d}{dx} & S(z) \end{bmatrix}$$

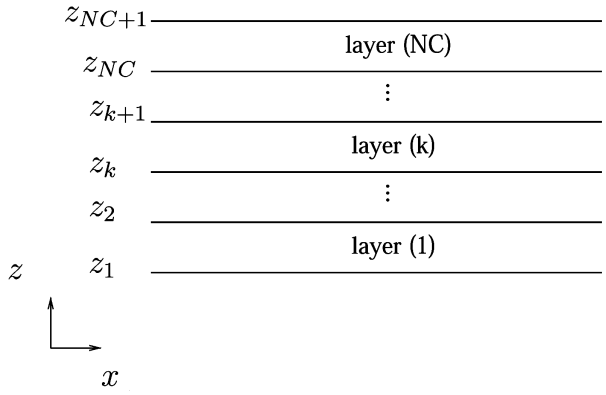

Fig. 2 coordinate system of laminated beam

3.4 The Layer-Wise Theory for Electric Potential

Based on successful experiences of Sheikh *et al*. [17], Cho and Oh [31-33], and Topdar *et al*. [34] in assuming piecewise linear electric potential along the transverse direction, linear electric potential has been used in this study. Therefore, electric potential anywhere in the *i*th layer can be expressed as

$$\phi(x,\ z,\ i\text{th layer}) = \phi_i(x)\ L_{id}(z) + \phi_{i+1}(x)\ L_{iu}(z) \tag{17}$$

where

$$L_{id}(z) = \frac{z - z_{i+1}}{z_i - z_{i+1}}\ ,\ \ L_{iu}(z) = \frac{z - z_i}{z_{i+1} - z_i}$$

and $\phi_i(x)$ and $\phi_{i+1}(x)$ are potential functions at the *i*th and $(i + 1)$th interfaces respectively.

The electric field can be derived from usual definition of electric field (see Eq. (6)):

$$E_i = \begin{bmatrix} E_x \\ E_z \end{bmatrix}_{layer\ i} = -\begin{Bmatrix} -\dfrac{\partial\phi}{\partial x} \\ -\dfrac{\partial\phi}{\partial z} \end{Bmatrix}_i$$
$$= -\begin{bmatrix} L_{id}(z)\dfrac{d}{dx} & L_{iu}(z)\dfrac{d}{dx} \\ \dfrac{dL_{id}(z)}{dz} & \dfrac{dL_{iu}(z)}{dz} \end{bmatrix} \begin{Bmatrix} \phi_i(x) \\ \phi_{i+1}(x) \end{Bmatrix} = -L_\phi^i\, u_\phi^{\ i} \tag{18}$$

4. FINITE ELEMENT FORMULATION

The mechanical and electrical elements being considered have been shown in Fig. 3. The three mechanical variables u_u can be expressed using four mechanical nodal variables u_u^e as follows:

$$u_u = N_u\, u_u^e \tag{19}$$

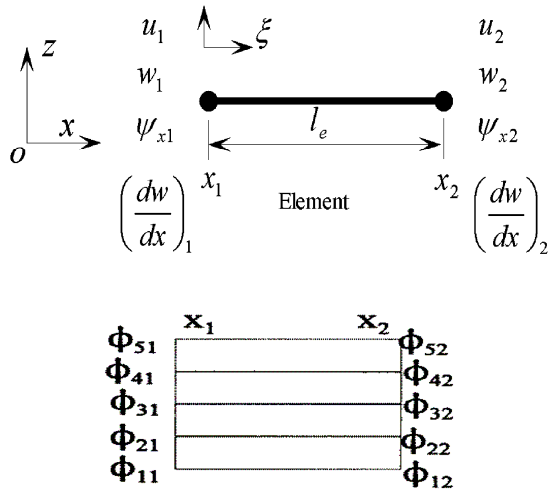

Fig. 3 (a) Mechanical two-nodded beam element; (b) Electrical five-nodded layer-wise element

where
$u_u^e = \{u_1\ w_1\ \psi_{x1}\ (dw/dx)_1\ u_2\ w_2\ \psi_{x2}\ (dw/dx)_2\}^T$,
shape function matrixin which N_1^0, N_2^0 are the Lagrangian shape functions defined as:

$$N_1^0 = N_1^0(\xi) = (1-\xi)/2\ ,\quad N_2^0 = N_2^0(\xi) = (1+\xi)/2 \tag{20}$$

and the Hermitian shape functions are

$$N_1 = N_1(\xi) = \frac{1}{4}(1-\xi)^2(2+\xi)\ ,$$
$$N_2 = N_2(\xi) = \frac{1}{4}(2-\xi)(1+\xi)^2$$
$$N_1' = N_1'(\xi) = \frac{1}{4}(1-\xi)^2(1+\xi)\ ,$$
$$N_2' = N_2'(\xi) = -\frac{1}{4}(1-\xi)(1+\xi)^2 \tag{21}$$

where ξ is the local coordinate defined as:

$$\xi = 2\frac{x-x_1}{x_2-x_1} - 1 \tag{22}$$

Using Eqs. (19) and (16), the displacements vector and the strain vector can be expressed as follows:

$$u = A_u\, u_u = A_u\, N_u\, u_u^e = N u_u^e\ ,$$
$$\varepsilon = L_u\, u_u = L_u\, N_u\, u_u^e = B_u\, u_u^e \tag{23}$$

where the N and B_u are the displacement interpolation matrix and strain interpolation matrix respectively.

The vector u_ϕ can be written as:

$$u_\phi = N_\phi\, u_\phi^e \tag{24}$$

where $N_\phi = \begin{bmatrix} N_1^0 & 0 & N_2^0 & 0 \\ 0 & N_1^0 & 0 & N_2^0 \end{bmatrix}$ and $u_\phi^e = [\phi_{i1}\ \ \phi_{(i+1)1}\ \ \phi_{i2}\ \ \phi_{(i+1)2}]$

From Eqs. (18) and (24), the electric field E can be expressed as:

$$E = -L_\phi\, u_\phi = -L_\phi\, N_\phi\, u_\phi^e = -B_\phi\, u_\phi^e \tag{25}$$

Substituting Eq. (13) and Eqs. (23) ~ (25) into Eq. (11) and assembling the element equations yields general dynamic equation of motion:

$$\therefore \begin{bmatrix} [M] & 0 \\ 0 & 0 \end{bmatrix} \begin{bmatrix} [\ddot{u}_u] \\ [\ddot{u}_\phi] \end{bmatrix} + \begin{bmatrix} [K_{uu}] & [K_{u\phi}] \\ [K_{\phi u}] & [K_{\phi\phi}] \end{bmatrix} \begin{bmatrix} [u_u] \\ [u_\phi] \end{bmatrix} = \begin{bmatrix} [F_u] \\ [F_\phi] \end{bmatrix} \tag{26}$$

The matrices and vectors in the above equation are the mass matrix $M = \int_V \rho N^T N\, dV$, the elastic matrix $K_{uu} = \int_V B_u^T \bar{C} B_u\, dV$, electromechanical coupling matrix $K_{u\phi} = \int_V B_u^T \bar{e} B_\phi\, dV$, the permittivity matrix $K_{\phi\phi} = \int_V B_\phi^T \bar{\chi} B_\phi\, dV$, the mechanical load vector $F_u = \int_V N^T f\, dV + \int_S N^T F\, dS + N^T f_c$ and the applied charge vector $F_\phi = \int_S N_\phi^T Q\, dS$.

5. NUMERICAL RESULTS

In order to validate the proposed model, the obtained numerical results have been compared with the experimental and numerical results of other researchers. The following case studies have been considered:

(i) Three-layer cantilever beam made of piezoelectric and non-piezoelectric materials.

(ii) PVDF bimorph beam.

The numerical results are obtained from a MATLAB program whose algorithm is based on the proposed model described in the previous sections. In the following case studies, the polarization of the piezoelectric layers is aligned in the transverse direction of these layers unless stated otherwise.

5.1 Three-Layer Cantilever Beam Made of Piezoelectric and Non-Piezoelectric Materials

The top and middle layer of this three layered cantilever beam is respectively made of piezoelectric material and adhesive. Its bottom layer (substrate) is isotropic aluminum or Gr/epoxy composite T300/934. However, we have used both materials for the bottom layer for comparison purposes. The geometric data and material properties of this beam have been shown in Table 1. This layered structure has bean studied by Saravanos and Heyliger [35], and Chee *et al*. [28].

Case I (Three-layer active cantilever): In this section, the actuator capability has been investigated. By applying a 12.5kV voltage across the thickness direction, the piezoelectric layer will act as an actuator, which will bend the beam. As shown in Fig. 4, this beam has been modeled by using five elements of equal length and four layers. Due to the existence of potential

Table 1 Properties for three-layer cantilever (data obtained from [28])

	Alumi-num	T300/934	Adhesive	PZT-4	
E_{11}	6.8900×10^{10}	1.3238×10^{11}	6.9000×10^{9}	8.1300×10^{10}	Pa
E_{33}	6.8900×10^{10}	1.0760×10^{10}	6.9000×10^{9}	6.4500×10^{10}	Pa
Poisson ratio 13	0.25	0.24	0.4	0.43	–
G_{13}	2.7600×10^{10}	5.6500×10^{10}	2.4600×10^{9}	2.5600×10^{10}	Pa
D_{31}	–	–	–	-1.22×10^{-10}	MV^{-1}
Elec. Perm. χ_{11}	–	3.0989×10^{-11}	–	1.305965×10^{-8}	FV^{-1}
Elec. Perm. χ_{33}	–	2.6562×10^{-11}	–	1.15102×10^{-8}	FV^{-1}
Length L	0.1524	0.1524	0.1524	0.1524	M
Thickness h	0.01524	0.01524	0.000254	0.001524	m
Width b	0.0254	0.0254	0.0254	0.0254	m

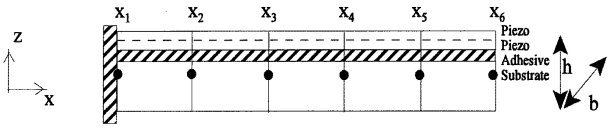

Fig. 4 Three-layer actuator/sensor cantilever beam

differences across the piezoelectric thickness, piezoelectric layer is divided into two layers. The obtained results from the present method have been compared with results from other researchers in Fig. 5. The proposed model, which ensures continuity condition for the transverse shear stresses, has a high agreement with mixed model of Chee *et al*.

Case II (Three-layer active/sensory cantilever): In order to investigate the sensory capability, a mechanical load of 1000N upwards was applied to the free tip of layered beam. Due to the electro-mechanical properties, a potential difference will appear across the thickness of piezoelectric layer. The mid-plane deflections along the beam and the total voltage across the thickness of the piezoelectric have been plotted in Figs. 6 and 7, respectively. From these figures, the deflection and the voltage distribution predicted by the present formulation have a very good correlation with results of Chee *et al*. [28].

5.2 PVDF Bimorph Beam

The second case study is a cantilever piezoelectric bimorph beam with two PVDF layers bonded together and polarized in opposite directions. This particular example and its related dimensions have been shown in Fig. 8. This bimorph beam has been studied by the following researchers: Hwang and Park [36], Tzou and Ye [37], Chee *et al*. [28], Tzou and Tseng [9], Suleman and Venkayya [38], Correia *et al*. [39], and Fukunaga *et al*. [40].

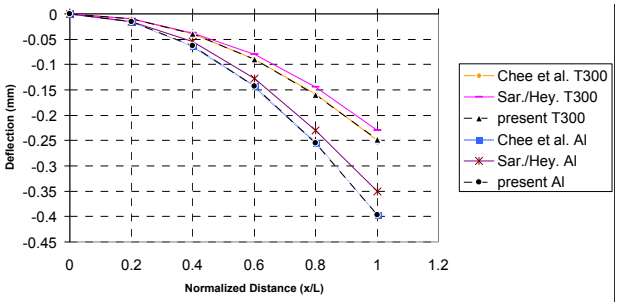

Fig. 5 Deflection induced by piezoelectric layer along the normalized length of the cantilever

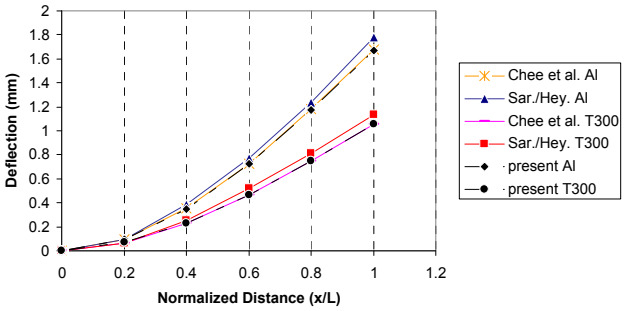

Fig. 6 Deflection due to load at cantilever tip

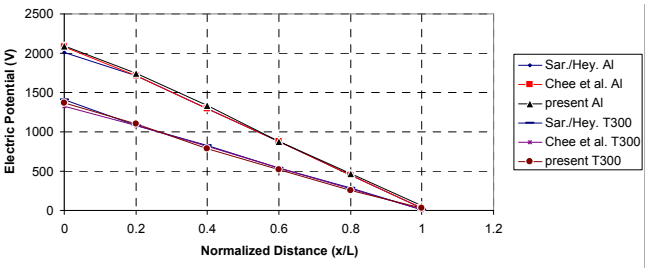

Fig. 7 Voltage difference across the piezoelectric layer

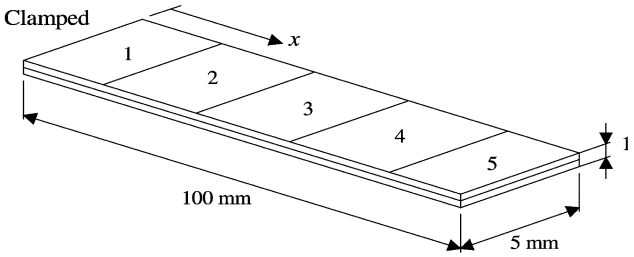

Fig. 8 Piezoelectric bimorph beam

In order to compare the present results with results obtained by these researchers, the following mechanical and piezoelectric properties are used for the PVDF beam: $E_{11} = E_{22} = E_{33} = 2$GPa, $G_{12} = G_{13} = G_{23} = 1$GPa, $\nu_{12} = \nu_{23} = \nu_{13} = 0.0$, $e_{31} = e_{32} = 0.0460 C/m^2$, and $\chi_{11} = \chi_{33} = 0.1062 \times 10^{-9}$F/m. The e_{33} coefficient is assumed to be zero. Also the beam has been discretized into five equal elements for comparison purposes.

Case I (Actuator model): By applying a total $1V$ voltage across the thickness direction, PVDF bimorph beam will act as an actuator. The induced deflections can be found in Table 2. For comparison, the results

Table 2 Comparison of deflections induced by actuators

	Deflections	(10^{-4} mm)			
Location x (mm)	20	40	60	80	100
Present	0.138	0.552	1.242	2.208	3.45
Mixed model (Chee *et al.* (1999))	0.138	0.552	1.242	2.208	3.45
Plate FE (nine-node element) (Fukunaga *et al.* (2001))	0.139	0.553	1.24	2.21	3.45
Plate FE (four-node element) (Fukunaga *et al.* (2001))	0.139	0.553	1.24	2.21	3.45
Theory (Tzou and Tseng (1990))	0.138	0.552	1.24	2.21	3.45
Plate FE (11 DOFs) (Correia *et al.* (2000))	0.138	0.552	1.24	2.21	3.45
Plate FE (9 DOFs) (Correia *et al.* (2000))	0.138	0.552	1.24	2.21	3.45
Shell FE (FDST) (Tzou and Ye (1996))	0.132	0.528	1.19	2.11	3.30
Plate FE (FDST) (Suleman and Venkaya (1995))	0.14	0.55	1.24	2.21	3.45
Analytical (Correia *et al.* (2000))	0.13	0.51	1.14	2.02	3.16
Experimental (Tzou and Tseng (1990))	–	–	–	–	3.15

obtained from Chee *et al*. [28], Tzou and Ye [37], Tzou and Tseng [9], Suleman and Venkaya [38], Correia *et al*. [39], and Fukunaga *et al*. [40] have been employed. From this table, it can be found that the present results are in very good agreement with previous theoretical and experimental results.

Case II (Sensor model): The sensor capability has been investigated in this section. The voltage distribution for an imposed tip deflection of 10mm has been plotted in Fig. 9. In this figure, the present results have been compared with the results obtained from Hwang and Park [36], Chee *et al*. [28], and Tzou and Tseng [9]. Because Hwang and Park used five pieces of separate electrode, the sensor voltage in Fig. 9 has a step distribution. However, it is possible to measure the sensor voltage using point electrodes. Measuring the sensor voltages via these types of electrodes leads to a sensor distribution as shown by the results of Tzou *et al*., Chee *et al*. and the present model. Figure 9 also indicates a good agreement between previous results and the present model.

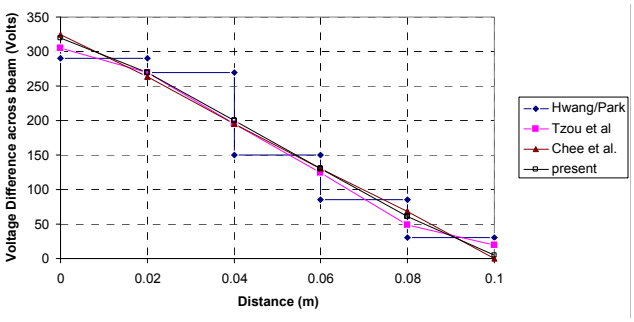

Fig. 9 Voltage difference across the thickness of PVDF along the length of the cantilever

6. CONCLUSIONS

In the present paper, finite element modeling of piezoelectric composite beams with distributed sensor and actuator layers is considered. The variation of mechanical displacement across the thickness has been modeled by a sinus model which ensures continuity condition for the transverse shear stresses as well as the boundary conditions on the upper and lower surfaces of the beam. Any piezoelectric layer in the laminated structure can function as sensor or actuator. This model has the distinct advantage of involving unknowns at the beam mid-plane only. For the electrical potential, the through thickness variation was modeled by the layer-wise theory. The proposed element has the three independent generalized displacements: Two displacements and one rotation. It has C^0 continuity, except for the transverse displacement which has C^1.

A three-layer cantilever beam made of piezoelectric and non-piezoelectric materials and a PVDF bimorph beam have been employed for validation. A computer code whose algorithm is based on the present model has been developed. Comparison of numerical results from this formulation with other published results shows that the present modeling method is suitable in predicting the behavior of laminated beams under mechanical and electrical loadings.

APPENDIX A

SINUS MODEL WITH CONTINUITY CONDITIONS [29]

A.1 Displacement Field

The beam displacement field is defined as follows:

$$u(x,\ z) = u(x) + zv(x) + f(z)\ u_2(x) + g(z)\ v_2(x) + \sum_{i=1}^{(NC)-1} u_i^c(x)(z - z_{i+1})\ H(z - z_{i+1})$$
$$w(x,\ z) = w(x) \tag{A.1}$$

where $u(x)$, $v(x)$, $u_2(x)$, $v_2(x)$, $u_i^c(x)$, $w(x)$ are the unknown functions. H is the Heaviside function, $f(z)$ and $g(z)$ are defined by

$$\begin{cases} f(z) = \dfrac{h}{\pi}\sin\left(\dfrac{\pi z}{h}\right) \\ f'(z) = \cos\left(\dfrac{\pi z}{h}\right) \end{cases} \qquad \begin{cases} g(z) = \dfrac{h}{\pi}\cos\left(\dfrac{\pi z}{h}\right) \\ g'(z) = -\sin\left(\dfrac{\pi z}{h}\right) \end{cases}$$

The transverse shear strain component can be written as:

$$\gamma_{13}(x,\ z) = v(x) + w'(x) + f'(z)\ u_2(x) + g'(x)\ v_2(x) + \sum_{i=1}^{(NC)-1} u_i^c(x)\ H(z - z_{i+1}) \tag{A.2}$$

A.2 Boundary Conditions

At the bottom surface $z_1 = -h/2$; the following relation must be satisfied:

$$\begin{aligned}\sigma_{13}^{(1)}(z_1) = 0 &\Leftrightarrow G^{(1)}\left(v(x) + w'(x) + v_2(x)\right) = 0 \\ &\Leftrightarrow v(x) + w'(x) = -v_2(x)\end{aligned} \tag{A.3}$$

In the same way, at the top surface $z_{NC+1} = h/2$; we have:

$$\begin{aligned}&\sigma_{13}^{(NC)}(z = z_{NC+1}) = 0 \\ &\Leftrightarrow G^{(NC)}\left(v(x) + w'(x) - v_2(x) + \sum_{i=1}^{(NC)-1} u_i^c(x)\right) = 0 \\ &\Leftrightarrow \sum_{i=1}^{(NC)-1} u_i^c = 2v_2(x)\end{aligned} \tag{A.4}$$

Then, the following relations can be deduced:

$$\begin{aligned}v(x) &= -w'(x) - \frac{1}{2}\sum_{i=1}^{(NC)-1} u_i^c(x) \\ v_2(x) &= \frac{1}{2}\sum_{i=1}^{(NC)-1} u_i^c(x)\end{aligned} \tag{A.5}$$

Substituting Eq. (A.5) in Eq. (A.1), the beam displacement field can be rewritten as:

$$\begin{aligned}&u(x,\ z) = u(x) - zw'(x) + u_2(x) f(z) \\ &\sum_{i=1}^{(NC)-1} u_i^c\left(-\frac{1}{2}z + \frac{1}{2}g(z) + (z - z_{i+1})H(z - z_{i+1})\right) \\ &w(x,\ z) = w(x)\end{aligned} \tag{A.6}$$

Unknown functions are now used to ensure the continuity conditions at each layer interface.

A.3 Continuity Conditions for the Transverse Shear Stress

From Eq. (A.6), the transverse shear strain can be expressed as:

$$\gamma_{13}(x,\ z) = f'(z)\ u_2(x) + \sum_{i=1}^{(NC)-1} u_i^c(x)\left(-\frac{1}{2} + \frac{1}{2}g'(z)\right) + \sum_{i=1}^{(NC)-1} u_i^c(x)\ H(z - z_{i+1}) \tag{A.7}$$

In order to ensure continuity condition for the transverse shear stress, we must have:

$$\sigma_{13}^{(k)}(z = z_{k+1}) = \sigma_{13}^{(k+1)}(z = z_{k+1}) \tag{A.8}$$

layer (k) :

$$\sigma_{13}^{(k)}(z_{k+1}) = G^{(k)}\left(f'(z_{k+1})\ u_2(x) + \frac{1}{2}\sum_{i=1}^{(NC)-1} u_i^c(x)\left(g'(z_{k+1}) - 1\right) + \sum_{i=1}^{k-1} u_i^c(x)\right)$$

layer ($k + 1$):

$$\sigma_{13}^{(k+1)}(z_{k+1}) = G^{(k+1)}\left(f'(z_{k+1})\ u_2(x) + \frac{1}{2}\sum_{i=1}^{(NC)-1} u_i^c(x) \times\left(g'(z_{k+1}) - 1\right) + \sum_{i=1}^{k-1} u_i^c(x) + u_k^c(x)\right)$$

For $k \in \{1,\ NC - 1\}$, Eq. (A.8) gives:

$$\begin{aligned}&G^{(k)}\left(f'(z_{k+1})\ u_2(x) + \frac{1}{2}\sum_{i=1}^{(NC)-1} u_i^c(x)\left(g'(z_{k+1}) - 1\right) + \sum_{i=1}^{k-1} u_i^c(x)\right) = G^{(k+1)}\left(f'(z_{k+1})\ u_2(x)\right. \\ &\left. + \frac{1}{2}\sum_{i=1}^{(NC)-1} u_i^c(x)\left(g'(z_{k+1}) - 1\right) + \sum_{i=1}^{k-1} u_i^c(x) + u_k^c(x)\right)\end{aligned} \tag{A.9}$$

Equation (A.9) can be written under the following form:

$$\begin{aligned}&(G^{(k)} - G^{(k+1)}) f'(z_{k+1})\ u_2 \\ &= G^{(k+1)} u_k^c(x) + (G^{(k+1)} - G^{(k)}) \\ &\times\left(\frac{1}{2}\sum_{i=1}^{(NC)-1} u_i^c(x)\left(g'(z_{k+1}) - 1\right) + \sum_{i=1}^{k-1} u_i^c(x)\right)\end{aligned} \tag{A.10}$$

Finally, a system of NC–1 equations is obtained for the NC–1 unknown functions $u_i^c(x)$. This system can be expressed as:

$$[A][U] = [B]\ u_2$$

where $[U]^t = [u_1^c\ u_2^c\ .....\ u_{NC-1}^c]$ and the coefficients A_{kl} of $[A]$ for $k \in \{1,\ NC–1\}$ are:

$$\begin{aligned}&l < k:\ A_{kl} = \left(G^{(k+1)} - G^{(k)}\right)\left(g'(z_{k+1}) + 1\right) \\ &l = k:\ A_{kl} = G^{(k)} + G^{(k+1)} + \left(G^{(k+1)} - G^{(k)}\right) g'(z_{k+1}) \\ &l > k:\ A_{kl} = \left(G^{(k+1)} - G^{(k)}\right)\left(g'(z_{k+1}) - 1\right)\end{aligned}$$

while $[B]$ is defined by coefficients:

$$B_k = 2\left(G^{(k)} - G^{(k+1)}\right) f'(z_{k+1})$$

The solution of this system yields $u_i^c(x) = \alpha_i\ u_2(x)$ where coefficients α_i are expressed from

$\left(G^{(k)}\right)_{k=1,NC}$; $\left(z_{k+1};\ g'(z_{k+1});\ f'(z_{k+1})\right)_{k=1,NC-1}$.

A.4 Final Displacement Field

The final displacement field takes the following form

$$u(x,\ z) = u(x) - zw'(x) + u_2(x)f(z) \sum_{i=1}^{(NC)-1} \alpha_i \left(-\frac{1}{2}z + \frac{1}{2}g(z) + (z - z_{i+1})H(z - z_{i+1}) \right) \tag{A.11}$$

$$w(x,\ z) = w(x)$$

Note that in the above equations $u_2(x) = \psi_x(x) + w'(x)$

REFERENCES

1. Crawley, E. F. and Luis, J., "Use of Piezoelectric Actuators as Element of Intelligent Structures," *American Institute of Aeronautics and Astronautics,* **25**, pp. 1373–1385 (1987).
2. Tzou, H. S. and Grade, M., "Theoretical Analysis of a Multi-Layered Thin Shell Coupled with Piezoelectric Shell Actuators for Distributed Vibration Controls," *Journal of Sound and Vibration*, **132**, pp. 433–450 (1989).
3. Wang, B. T. and Rogers, C. A., "Laminate Plate Theory for Spatially Distributed Induced Strain Actuators," *Journal of Composite Materials*, **25**, pp. 433–425 (1991).
4. Sung, C. K., Chen, T. F. and Chen, S. G., "Piezoelectric Modal Sensor/Actuator Design for Monitoring /Generating Flexural and Torsional Vibrations of Cylindrical Shells," *Journal of Sound and Vibration*, **118,** pp. 48–55 (1996).
5. Wu, C. P., Syu, Y. S. and Lo, J. Y., "Three-Dimensional Solutions for Multilayered Piezoelectric Hollow Cylinders by an Asymptotic Approach," *International Journal of Mechanical Sciences,* **49**, pp. 669–689 (2007).
6. Wu, C. P. and Liu, K. Y., "A State Space Approach for the Analysis of Doubly Curved Functionally Graded Elastic and Piezoelectric Shells," *Computers, Materials and Continua,* **6**, pp. 144–199 (2007).
7. Wu, C. P., Chiu, K. H. and Wang, Y. M., "A Review on the Three-Dimensional Analytical Approaches of Multilayered and Functionally Graded Piezoelectric Plates and Shells," *Computers, Materials and Continua,* **18**, pp. 93–132 (2008).
8. Allik, H. and Hughes, T. J. R., "Finite Element Method for Piezoelectric Vibration," *International Journal for Numerical Methods in Engineering*, **2**, pp. 151–157 (1970).
9. Tzou, T. S. and Tseng, C. I., "Distributed Piezoelectric Sensor/Actuator Design for Dynamic Measurement /Control of Distributed Parameter System: A Piezoelectric Finite Element Approach," *Journal of Sound and Vibration*, **138**, pp. 17–34 (1990).
10. Xu, K. M., Noor, A. K. and Tang, Y., "Three-Dimensional Solutions for Coupled Thermo-Electro-Elastic Response of Multi-Layered Plates," *Computer Methods in Applied Mechanics and Engineering,* **126**, pp. 355–371 (1995).
11. Semedo Garcao, J. E., Mota Soares, C. M., Mota Soares, C. A. and Reddy, J. N., "Analysis of Laminated Adaptive Plate Structures Using Layer-Wise Finite Element Models," *Composite Structures,* **82**, pp. 1939–1959 (2004).
12. Garcia Lage, R., Mota Soares, C. M., Mota Soares, C. A. and Reddy, J. N., "Analysis of Laminated Adaptive Plate Structures by Mixed Layer-Wise Finite Element Models," *Composite Structures,* **66**, pp. 269–276 (2004).
13. Garcia Lage, R., Mota Soares, C. M., Mota Soares, C. A. and Reddy, J. N., "Modeling of Piezolaminated Plates Using Layer-Wise Mixed Finite Element Models," *Composite Structures,* **82,** pp. 1849–1863 (2004).
14. Heyliger, P. R. and Saravanos, D. A., "Coupled Discrete-Layer Finite Elements for Laminated Piezoelectric Plates," *Communications in Numerical Methods in Engineering,* **10**, pp. 971–981 (1994).
15. Saravanos, D. A., Heyliger, P. R. and Hopkins, D. A., "Layer-Wise Mechanics and Finite Element Model for the Dynamic Analysis of Piezoelectric Composite Plates," *International Journal of Solids and Structures,* **34**, pp. 359–378 (1997).
16. Mitchell, J. A. and Reddy, J. N., "A Refined Plate Theory for Composite Laminates with Piezoelectric Laminate," *International Journal of Solids and Structures,* **32**, pp. 2345–2367 (1995).
17. Sheikh, A. H., Topdar, P. and Halder, S., "An Appropriate FE Model for Through Thickness Variation of Displacement and Potential in Thin/Moderately Thick Smart Laminates," *Composite Structures,* **51**, pp. 401–409 (2001).
18. Carrera, E., "Theories and Finite Elements for Multilayered, Anisotropic, Composite Plates and Shells," *Archives of Computational Methods in Engineering,* **9**, pp. 87–140 (2002).
19. Noor, A. K. and Burton, W. S., "Assessment of Shear Deformation Theories for Multilayered Composite Plates," *Applied Mechanics Reviews,* **42**, pp. 1–13 (1989).
20. Reddy, J. N., and Robbins, D. H. Jr., "Theories and Computational Models for Composite Laminates," *Applied Mechanics Reviews,* **47** Part 1, pp. 147–169 (1994).
21. Di Sciuva, M., "A Refined Transverse Shear Deformation Theory for Multilayered Anisotropic Plates," *Atti Accademia Scienze Torino,* **118**, pp. 279–295 (1984).
22. Lue, D. and Li, X., "An Overall View of Laminate Theories Based on Displacement Hypothesis," *Journal of Composite Materials*, **30**, pp. 1539–1560 (1996).
23. Bhaskar, K. and Varadan, T. K., "Refinement of Higher Order Laminated Plate Theories," *American Institute of Aeronautics and Astronautics,* **27**, pp. 1830–1831

(1989).

24. Di Sciuva, M., "Multilayered Anisotropic Plate Models with Continuous Interlaminar Stress," *Computers and Structures,* **22**, pp. 149–167 (1992).
25. Lee, C. Y. and Liu, D., "Interlaminar Shear Stress Continuity Theory for Laminated Composite Plates," *American Institute of Aeronautics and Astronautics,* **29**, pp. 2010–2012 (1991).
26. Cho, M. and Parmerter, R. R., "Efficient Higher Order Plate Theory for General Lamination Configurations," *American Institute of Aeronautics and Astronautics,* **31,** pp. 1299–1308 (1993).
27. Reddy, J. N., "A Simple Higher-Order Theory for Laminated Composites," *Journal of Applied Mechanics, Transactions of the ASME,* **51**, pp. 745–752 (1984).
28. Chee, C. Y. K., Tong, L. and Steven, P. G., "A Mixed Model for Composite Beams with Piezoelectric Actuators and Sensors," *Smart Materials and Structures,* **8**, pp. 417–432 (1999).
29. Vidal, P. and Polit, O., "A Family of Sinus Finite Elements for the Analysis of Rectangular Laminated Beams," *Composite Structures,* **84**, pp. 56–72 (2008).
30. Benjeddou, A., "Advances in Piezoelectric Finite Element Modeling of Adaptive Structural Elements: A Survey," *Computers and Structures,* **76**, pp. 347–363 (2000).
31. Cho, M. and Oh, J., "Higher Order Zig-Zag Plate Theory Under Thermo-Electric-Mechanical Loads Combined," *Composites Part B: Engineering,* **34**, pp. 67–82 (2003).
32. Cho, M. and Oh, J., "Higher Order Zig-Zag Theory for Fully Coupled Thermo-Electric-Mechanical Smart Composite Plates," *International Journal of Solids and Structures*, **41**, pp. 1331–1356 (2004).
33. Oh, J. and Cho, M., "A finite Element Based on Cubic Zig-Zag Plate Theory for the Prediction of Thermo-Electric-Mechanical Behaviors," *International Journal of Solids and Structures*, **41**, pp. 1357–1375 (2004).
34. Topdar, P., Chakraborti, A. and Sheikh, A. H., "An Efficient Hybrid Plate Model for Analysis and Control of Smart Sandwich Laminates," *Computer Methods in Applied Mechanics and Engineering,* **193**, pp. 4591–4610 (2004).
35. Saravanos, D. A. and Heyliger, P. R., "Coupled Layer-Wise Analysis of Composite Beams with Embedded Piezoelectric Sensors and Actuators," *Journal of Intelligent Material Systems and Structures,* **6**, pp. 350–363 (1995).
36. Hwang, W. S. and Park, H. C., "Finite Element Modeling of Piezoelectric Sensors and Actuators," *American Institute of Aeronautics and Astronautics,* **31**, pp. 930–937 (1993).
37. Tzou, H. S. and Ye, R., "Analysis of Piezoelastic Structures with Laminated Piezoelectric Triangle Shell Elements," *American Institute of Aeronautics and Astronautics,* **34**, pp. 110–115 (1996).
38. Suleman, A. and Venkaya, V. B., "A Simple Finite Element Formulation for a Laminated Composite Plate with Piezoelectric Layers," *Journal of Intelligent Material Systems and Structures,* **6**, pp. 776–782 (1995).
39. Correia, F. V. M., Gomes, M. A. A. and Suleman, A., "Modeling and Design of Adaptive Composite Structures," *Computer Methods in Applied Mechanics and Engineering,* **185**, pp. 325–346 (2000).
40. Fukunaga, H., Hu, N. and Ren, G. X., "Finite Element Modeling of Adaptive Composite Structures Using a Reduced Higher-Order Plate Theory via Penalty Functions," *International Journal of Solids and Structures*, **38**, pp. 8735–8752 (2001).

(Manuscript received April 24, 2009,
accepted for publication July 28, 2009.)